Advances in Translational Medicine
https://ojs.luminescience.cn/ATM

LUMINESCIENCE
https://luminescience.cn/

Review

Molecular nanoprobes for diagnosis of cardiovascular diseases

Chuang Wei[1#], Yin Wang[1,2,#], Peifeng Li[1*], Qinrui Fu[1,2*]

[1] Institute for Translational Medicine, The Affiliated Hospital of Qingdao University, College of Medicine, Qingdao University, Shandong Province, China.
[2] Key Laboratory of Birth Regulation and Control Technology of National Health Commission of China, Maternal and Child Health Care Hospital of Shandong Province affiliated to Qingdao University, Shandong Province, China.

[#] Chuang Wei and Yin Wang contributed equally to this work.
[*] Corresponding: Peifeng Li (peifli@hotmail.com); Qinrui Fu (fuqinrui2018@163.com)

Abstract:
Cardiovascular disease (CVD) is one of the most devastating diseases with high incidence and mortality worldwide. Early and accurate diagnosis is the key to effective therapy, and unequivocal identification of the atherosclerotic vulnerable plaques and infarcted myocardium may require advanced technologies and expertise. However, existing diagnostic approaches are currently at the infant stage of technological development. Emerging molecular imaging techniques possess the potential to enhance the understanding of CVD. Designing suitable molecular imaging probes is vital to the success of any molecular imaging study. Nanoparticles (NPs)-based biomedical imaging probes have been investigated extensively as potential alternatives to conventional molecular imaging probes. Herein, we first summarized the concepts and characteristics of different molecular imaging including fluorescence (FL) imaging, photoacoustic (PA) imaging, magnetic resonance imaging (MRI), ultrasound (US) imaging, computed tomography (CT) imaging, and multimodal imaging. And then we focused on the application of nanoprobes as contrast agents in molecular imaging of CVD, and finally briefly introduced the challenges and prospects of nanoprobes-based molecular imaging.

Keywords: Cardiovascular disease, Nanoprobe, Molecular imaging, Diagnosis

Introduction

Cardiovascular disease (CVD), including acute myocardial infarction (AMI) and atherosclerosis (AS), accounts for most of the deaths in the worldwide [1-5]. In etiology, long-term AS is caused by inflammation of blood vessels and fibrin deposition, which leads to blockage of blood vessels and eventually develops into loss of heart function [6-9]. Accurate and timely diagnosis may help facilitate earlier recovery, minimize early complications, and prevent further plaque formation. Despite this, early detection is difficult and late diagnosis is one of the major causes of poor prognosis and high mortality [10-14].

The current diagnostic methods for diagnosing CVD include biomarkers, electrocardiograms, and molecular imaging [15-19]. Concerning biomarkers, troponin I (cTnI) is considered the most robust biomarker in AMI, but in many cases its specificity is insufficient because it can be detected in non-CVD such as kidney injury [20-23]. The electrocardiogram has been used to assess cardiac abnormalities. However, electrocardiography may reveal nonspecific abnormalities in conduction or repolarization [24-28]. Therefore, molecular imaging becomes particularly important for CVD diagnosis.

In recent years, molecular imaging has received extensive

Received: Sep.23, 2022; Revised: Oct.24, 2022; Accepted: Nov.4, 2022; Published: Nov.7, 2022

DOI: https://doi.org/10.55976/atm.12022112661-76

attention because of its ability to non-invasively visualize and quantify the physio-pathological system at the cellular or molecular level, which can be summarized based on the existing literature [29-34]. Currently, molecular imaging mainly includes fluorescence (FL) imaging, photoacoustic (PA) imaging, magnetic resonance imaging (MRI), ultrasound (US) imaging, computed tomography (CT) imaging, and multimodal imaging [35-38]. Among them, molecular imaging agents play essential roles that may determine the final imaging effect. Molecular imaging agents are mainly divided into small molecules and nanoprobes [39, 40]. Despite their significant contributions to CVD diagnosis, a small molecule has inevitable limitations as molecular imaging agents because of rapid clearance, poor imaging adaptation, potential toxicity, and relatively weak signal intensity [41, 42]. These limitations have led to the development of nanoprobes-based molecular imaging. Compared with small molecules, nanoprobes may possess several significant advantages, such as aggregated emission signals, prolonged residence time, enhanced penetration, high surface area/volume ratio, and excellent adaptability [43- 46]. Indeed, nanoprobes-based molecular imaging has been widely applied in the diagnosis and image-guided therapy of CVD and other diseases, showing unlimited prospects.

While various molecular imaging probes have been reported for the diagnosis of CVD, to the best of our knowledge, an in-depth understanding of the use of nanoprobes as contrast agents in the diagnosis of CVD has rarely been summarized in the form of an imaging classification. Here we first introduced the concepts and features of various molecular imaging methods including FL imaging, PA imaging, MR imaging, US imaging, CT imaging, and multimodal imaging. Then, a comprehensive review of nanoprobes-based molecular imaging involved in the diagnosis of CVD was highlighted. Finally, we briefly mentioned the current challenges and future perspectives of nanoprobes-based molecular imaging in diagnosing CVD.

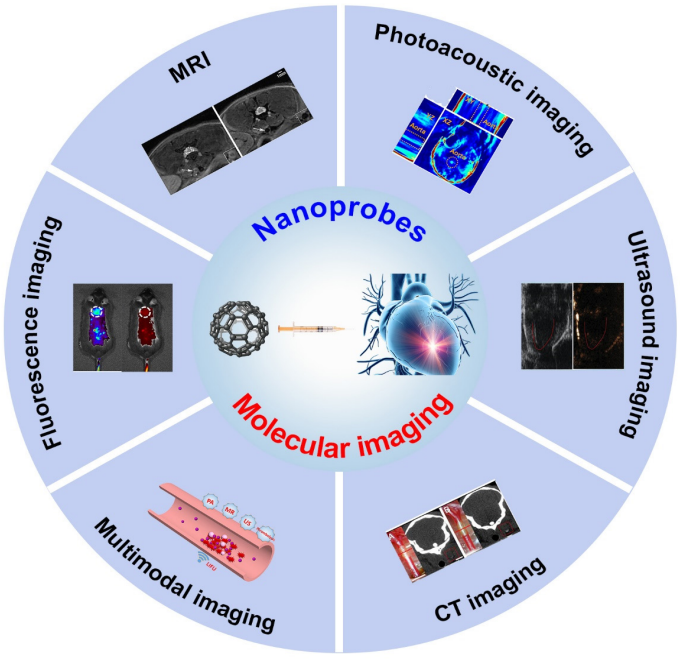

Scheme 1. Schematic illustration of molecular nanoprobes for imaging of cardiovascular diseases.

1. Molecular imaging

1.1 Fluorescence imaging

Fluorescence (FL) imaging is a noninvasive modality that detects photons emitted from fluorescent probes excited by a laser [47, 48]. FL imaging offers some excellent features over other imaging techniques, including cost efficiency, high sensitivity, facile detection, and the ability to adjust FL properties quickly [49-52]. For example, Li et al. developed a ROS-responsive core-shell bifunctional NPs (LFP/PCDPD NPs) consisting of plaque-targeted dextran as a shell and complex as a core for the theranostics of AS (Figure 1A) [53]. The complex was composed of lipid-specific aggregation-induced emission (AIE) FL probe (LFP), anti-inflammatory drug prednisolone (Pred) and lipid-removal cyclodextrin. The core and shell were connected by ROS-responsive poly (2-(methylthio) ethyl methacrylate) (PMEMA). In the presence of ROS, PMEMA was oxidatively cleaved, resulting in the release of the LFP, Pred and cyclodextrin. Because LFP was readily soluble in DMSO, the aggregation degree of LFP increased with the decrease of DMSO fraction in H_2O/DMSO mixed solution and the increased FL intensity with falling DMSO fraction confirmed the AIE properties of LFP (Figure 1B). Moreover,

upon H_2O_2 treatment, the FL wavelength of the oil solution of LFP/PCDPD was blue-shifted compared with that of the water solution of LFP/PCDPD and emitted FL changed from orange to green, suggesting that ROS-responsive LFP/PCDPD had lipid-specific FL imaging capability (Figure 1C). After incubation with lipid-enriched foam cells, the LFP/PCDPD accumulated significantly in foam cells and emitted distinct green FL at 495–540 nm (Figure 1D). However, after incubation with control RAW 264.7 cells, LFP/PCDPD emitted orange FL at 575–630 nm (Figure 1E). These results confirmed that the LFP/PCDPD possessed the capability of lipid-responsive FL imaging. After intravenous administration, due to the modification of the dextran, the LFP/PCDPD specifically accumulated in the ROS-enriched plaque area and released LFP, resulting in emitting the green FL in the aortic plaque area of mice instead of normal tissue. The results illustrated that the ROS-responsive and lipid-specific LFP/PCDPD enabled the diagnosis of AS (Figure 1F). This work showed the potential of nanoprobes as FL contrast agents.

Single biomarker responsive imaging easily leads to misdiagnosis due to false positive signals, while multiple biomarker responsive imaging helps to improve the accuracy and specificity of diseases diagnosis. Based on the premise that lipid accumulation and oxidative stress coexist in the atherosclerotic plaque area, Liu and co-workers prepared a dual-target sequentially activated fluorescent nanoprobe (iSHERLOCK) consisting of Boron-dipyrromethene (BODIPY) 493/503 as FL scaffold, lipophilic bis(trifluoromethyl) phenyl group (CF_3) as LD responsive moiety and 4-(methylthio)-benzaldehyde (MTB) as hypochlorous acid (HClO) reactive moiety for sequentially detecting LDs and HClO (two typical markers of AS) (Figure 1G) [54]. MTB and CF_3 were connected to BODIPY to synthesize a π-conjugated polymer with a donor (phenylthioether group) - acceptor (two trifluoromethyl groups) alternating copolymer structure (MTB-B-CF_3), which caused the excitation and emission wavelengths redshift to 561 and 615 nm respectively from 493 and 503 nm, and emitted FL due to intramolecular charge transfer (ICT) effect. However, because of the intermolecular aggregation-caused quenching (ACQ), the lipophilic probe exhibited a weak FL signal in aqueous solutions, whereas it showed a strong FL signal in LDs. The red FL at 670 nm (F_R) of MTB-B-CF_3 was increased as a function of LDM concentration due to the high affinity between MTB-B-CF_3 and TDM (LD mimetic) (Figure 1H). Furthermore, with the increasing HClO concentration, the FL of MTB-B-CF_3-LDM shifted from 615 nm to 600 nm (F_Y), along with a decrease at 670 nm, and accompanied by a change of FL from red to yellow (Figure 1I), thus showing an LD and HClO responsive FL ratiometric imaging (Y/R). After intravenous injection of MTB-B-CF_3, the higher FL signals (both red and yellow signals) and higher Y/R ratio signal in the aorta of AS model mice (ApoE$^{-/-}$ mice) instead of normal mice (C57BL/6J mice) was observed, while the Y/R ratio signal in the liver of both ApoE$^{-/-}$ mice and C57BL/6J mice was not significantly different (Figure 1J-L). The results demonstrated that the LD and HClO responsive probe with ratiometric FL imaging could effectively distinguish plaques to diagnose AS.

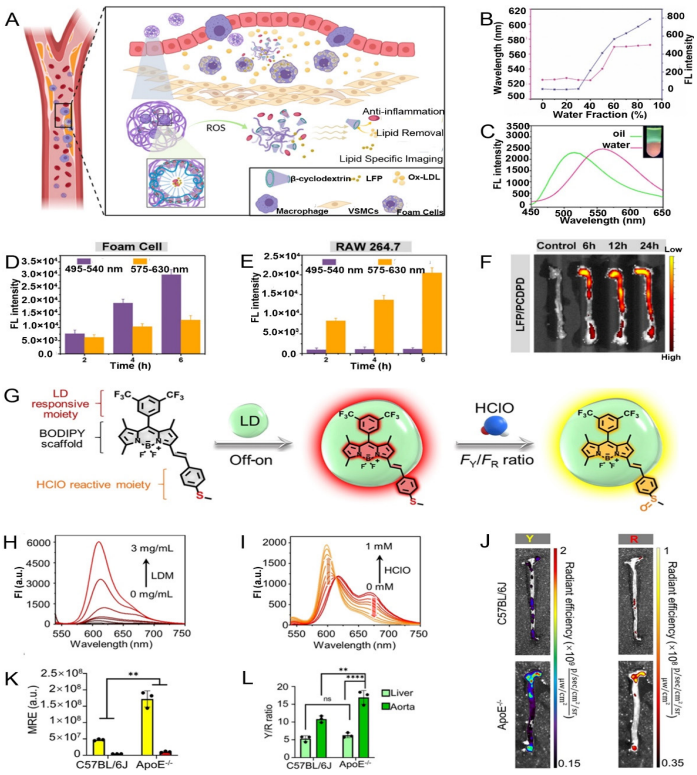

Figure 1. (A) Schematic illustration of ROS-responsive LFP/PCDPD. (B) Variation of FL emission wavelength and FL intensity of different DMSO fractions in H_2O/DMSO mixed solution. (C) FL spectra and photographs of LFP/PCDPD in water or oil after 1mM H_2O_2 treatment. (D) FL intensity after treatment of foam cells with LFP/PCDPD. (E) FL intensity after treatment of RAW 264.7 cells with LFP/PCDPD. (F) FL images of mouse aortas treated with LFP/PCDPD. (G) Schematic illustration of MTB-B-CF_3. (H) FL spectra of MTB-B-CF_3 treated with varying concentrations of LDM. (I) FL spectra of MTB-B-CF_3-LDM treated with different concentrations of HClO. (J) FL images of the aorta of different mice treated with MTB-B-CF_3 combined with Ac-LDL complexes. (K) FL mean radiation efficiency (MRE) of mice aorta. (L) Ratiometric Y/R values of aortas. (A-F) Reproduced with permission [53]. Copyright 2022, Elsevier. (G-L) Reproduced with permission [54]. Copyright 2022, Wiley-VCH.

1.2 Photoacoustic imaging

Photoacoustic imaging (PA) is a functional imaging technique based on the PA effect and US properties [55, 56]. The principle is that the contrast agent converts light energy into thermal energy, causing thermoelastic tissue expansion. Thermoelastic expansion generates acoustic waves, which are detected and converted into PA images by the instrument [57, 58]. Contrast agents are divided into endogenous (melanin, hemoglobin) and exogenous contrast agents (nanoprobes) [59, 60]. Although endogenous contrast agents can provide PA signals, poor near-infrared absorption of tissue limits the feedback of endogenous contrast agents to the tissue information, resulting in insufficient imaging depth and signal attenuation [61, 62]. Therefore, developing sensitive and specific exogenous contrast agents for PA imaging has received increasing attention. For example, Zheng et al. prepared a PA nanoprobe with the ability to target the vulnerable plaque (OPN Ab/Ti_3C_2/ICG) consisting of osteopontin antibody (OPN Ab) as a plaque targeting agent and Ti_3C_2 nanosheets loaded indocyanine green (ICG) as PA contrast agent for diagnosis of AS (Figure 2A) [63]. Ti_3C_2 nanosheets (Figure 2B) and ICG have excellent PA imaging performance, and the combination of the two significantly improves the PA imaging performance (Figure 2C). After intravenous injection, the OPN Ab/Ti_3C_2/ICG probe was specifically enriched in the atherosclerotic lesion area because of the modification of OPN, and exhibited a higher PA signal in AS mice compared to other groups (Figure 2D,E). Thus, the OPN Ab/Ti_3C_2/ICG-based PA probe enabled accurate AS diagnosis by PA imaging.

Recently, ratiometric PA imaging has been widely used for the diagnosis of diseases with its unique advantages, which can circumvent the absolute intensity-dependent signal readout inherent in conventional imaging and realize the built-in self-calibration of signal correction [64, 65]. For instance, Zhang and co-workers reported a semiconductor polymer nanomaterial (RSPN) consisting of hydrophobic $O_2^{\bullet-}$–responsive molecules, hydrophobic $O_2^{\bullet-}$–insensitive semiconducting polymer molecules, and amphiphilic polymers to detect $O_2^{\bullet-}$ level of AS plaques via ratiometric PA imaging (Figure 2F) [66]. An $O_2^{\bullet-}$ concentration-dependent enhanced PA signal at 690 nm was observed, while the signal at 800 nm remained stable, resulting in an $O_2^{\bullet-}$ concentration-dependent enhanced ratio of the PA_{690}/PA_{800}, which demonstrated RSPN could detect the concentration of $O_2^{\bullet-}$ through PA_{690}/PA_{800} ratio (Figure 2G,H). After the incubation of the RNSP with the cells, the PA_{690}/PA_{800} ratio of macrophages in the $O_2^{\bullet-}$ generation group was higher than that in the control group, illustrating that RSPN was an excellent ratiometric probe that can accurately reflect the $O_2^{\bullet-}$ concentration in macrophages through PA_{690}/PA_{800} ratio (Figure 2I). After intravenous administration of RSPN, the plaque-bearing mice group had a higher PA_{690}/PA_{800} ratio than that of the normal mice group. Meanwhile, the plaque-bearing mice group exhibited a lower PA_{690}/PA_{800} ratio than the plaque-bearing mice with the pneumonia group. The results demonstrated that RSPN could be used as a PA nanoprobe to distinguish plaque-bearing mice, plaque-bearing pneumonia mice, and healthy mice by assessing the content of $O_2^{\bullet-}$ in the plaques (Figure 2J,K). The results demonstrated that ratiometric PA imaging could accurately detect subtle differences in the target and exclude the interference of the plaque microenvironment, thereby improving the diagnostic accuracy of AS.

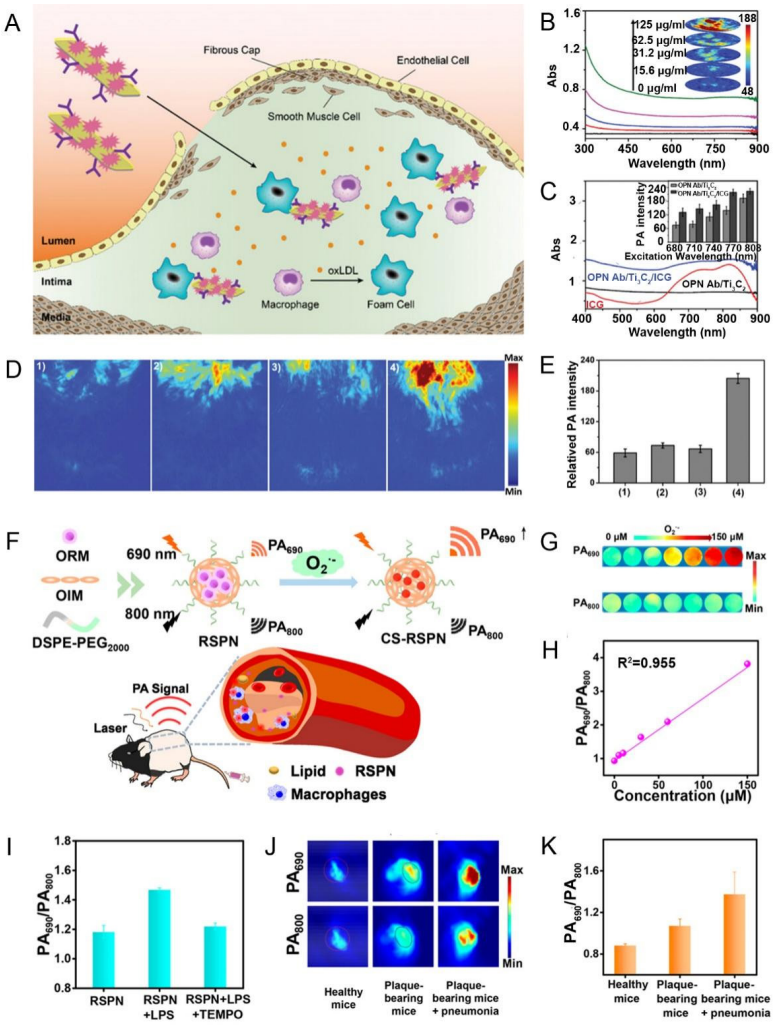

Figure 2. (A) Schematic illustration of OPN Ab/Ti_3C_2/ICG. (B) UV-Vis spectra of Ti_3C_2 nanosheets with different concentrations, and PA imaging of Ti_3C_2 nanosheets with 808 nm laser. (C) UV-Vis spectra and PA intensities of various nanosheets. (D) PA images of different mice. (E) PA intensity in different mice. Grouping: 1) AS model mice without treatment, 2) AS model mice intravenously injected with Ti_3C_2/ICG, 3) healthy C57BL/6J mice intravenously injected with OPN Ab/Ti_3C_2/ICG, 4) AS model mice intravenously injected with OPN Ab/Ti_3C_2/ICG. (F) Schematic illustration of RSPN. (G) PAI of two wavelengths at different $O_2^{\bullet-}$ concentrations. (H) Quantification of PA_{690}/PA_{800} ratios in solution. (I) Quantification of PA_{690}/PA_{800} ratios in RAW264.7 cells. (J) PA images in different mice after RSPN treatment. (K) Quantification of PA_{690}/PA_{800} ratios in different mice. (A-E) Reproduced with permission [63]. Copyright 2020, Wiley-VCH. (F-K) Reproduced with permission [66]. Copyright 2021, American Chemical Society.

1.3 Magnetic resonance imaging

Magnetic resonance (MR) imaging has been extensively employed among numerous clinical diagnostic techniques over the past two decades because of its safety and high spatial resolution [67-72]. For example, Hu et al. designed a magnetic nanoprobe (EGFP-EGF1-SPIONs) consisting of enhanced green fluorescent protein-first epidermal growth factor (EGFP-EGF1) as plaque-targeting agents and superparamagnetic iron oxide NPs (SPIONs) as MR contrast agents for the diagnosis of AS plaques (Figure 3A) [73]. The relaxation coefficient (r_2) of EGFP-EGF1-SPIONs was significantly higher than that of SPIONs, indicating that the targeted modification achieved the contrast enhancement of EGFP-EGF1-SPIONs (Figure 3B). Moreover, the T_2-weighted images of both NPs showed Fe concentration-dependent contrast enhancement, and the image of EGFP-EGF1-SPIONs was darker than that of SPIONs. These results confirmed the properties of EGFP-EGF1-SPIONs as MRI T_2 contrast agents. After intravenous administration, the MR signals intensities of the EGFP-EGF1-SPIONs-treated AS mice group were higher than that of the EGFP-EGF1-SPIONs-treated normal mice group (Figure 3C, D), indicating that EGFP-EGF1-SPIONs as powerful MR contrast agents could achieve an effective diagnosis of AS.

Thrombosis contributes to the rupture of plaques and clots in AS. MR imaging shows the promise not only for AS diagnosis, but also for thrombus [74, 75]. For example, Wang and co-workers designed an activated platelet-targeted NP (MFe_2O_4–ZnDPA) consisting of $Zn_{0.4}Co_{0.6}Fe_2O_4$@$Zn_{0.4}Mn_{0.6}Fe_2O_4$ as contrast agents and

Zn (II)-bis(dipicolylamine) as targeting agents for MR imaging of thrombus (Figure 3E) [76]. The rate of change in the T_2 signal increased with the increasing Fe concentration, confirming the MFe_2O_4–ZnDPA possessed excellent MR characteristic (Figure 3F). Furthermore, the T_2 signal of MFe_2O_4–ZnDPA in the activated platelets was significantly higher than that in the resting platelets, indicating that MFe_2O_4–ZnDPA NPs could specifically image activated platelets by MR imaging. After intravenous injection of different NPs into thrombus model rabbits, MFe_2O_4–ZnDPA NPs accumulated in the thrombus because of the modification of Zn (II)-bis(dipicolylamine), and the $T_{thrombus}$/ T_{water} signal ratio in the MFe_2O_4–ZnDPA group decreased from 0.67 to 0.05 within 15 minutes, while the changes in the other two groups were negligible, confirming that MFe_2O_4–ZnDPA can be an effective MR contrast agent for diagnosing thrombus (Figure 3G). These results highlighted the high efficacy of MR imaging in CVD diagnosis.

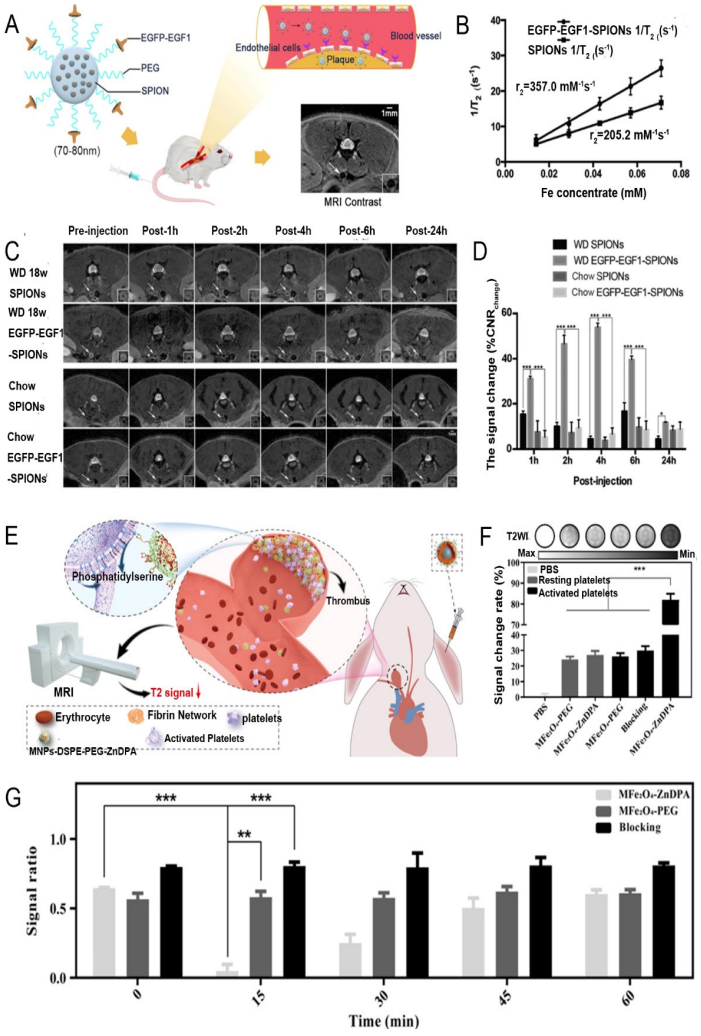

Figure 3. (A) Schematic illustration of EGFP-EGF1-SPIONs. (B) T_2 relaxation rate ($1/T_2$, S^{-1}) of different nanoprobes. (C) T_2-weighted MRI of the abdominal aorta in different mice treated with different nanoprobes. (D) Quantitative analysis of MRI signal changes. WD 18w: $ApoE^{-/-}$ mice were fed a high-fat diet for 18 weeks. WD 24w: $ApoE^{-/-}$ mice were fed a high-fat diet for 24 weeks. Chow group: C57 mice were fed with a normal diet for 18 weeks. (E) Schematic illustration of MFe_2O_4–ZnDPA. (F) MRI and signal change rates of two platelets after different NPs treatments. (G) signal ratio (T_t/T_w) of the thrombus. (A-D) Reproduced with permission [73]. Copyright 2019, Elsevier. (E-G) Reproduced with permission [76]. Copyright 2021, American Chemical Society.

1.4 Ultrasound imaging

Ultrasound (US) imaging is an effective, reliable, and convenient method for performing routine screening and monitoring examinations [77-79]. US imaging possesses various merits including high spatial and temporal resolution, no ionizing radiation, simple operation, rapid imaging, low cost, few side effects, and real-time data processing, which can serve as a promising diagnostic modality for CVD [80, 81]. For example, Zheng et al.

developed a triple-targeted nanomaterial (MB_{VIS}) consisting of vascular cell adhesion molecule 1 (VCAM-1) antibodies, intercellular adhesion molecule 1 (ICAM-1) antibodies, synthetic polymeric sialyl Lewis X (sLe^x), and microbubble (MB) as a US contrast agent for diagnosis of AS (Figure 4A) [82]. VCAM-1 antibodies, ICAM-1 antibodies and sLe^x were integrated into the surface of MB to enhance the targeting of MB to plaques. After intravenous injection of US contrast agents into AS model mice, the echo signal intensity (DTE) of the MB_{VIS} group was significantly higher than that of the control group (MB_{IgG}), the single targeting group (MB_V, MB_I, MB_S) and the double targeting group (MB_{VI}, MB_{VS}, MB_{IS}), suggesting MB_{VIS} possessed excellent US imaging capability due to the triple targeting modification (Figure 4B). After intravenous injection, compared with other groups, the echo intensity in AS model mice (A-HD) was significantly increased, and the intensity was positively correlated with the degree of lesions (time of high-fat diet feeding), indicating that MB_{VIS} could not only diagnose AS, but also identify the degree of the lesion (Figure 4C,D). This work showed the potential of US imaging in CVD diagnosis.

In another example, Guo and co-workers designed a liquid-gas phase transition NPs (Fe_3O_4-PLGA-PFH-CREKA) consisting of Fe_3O_4, poly (lactic-co-glycolic acid) (PLGA), perfluorohexane (PFH), and thrombus-targeted CREKA peptide for diagnosis and treatment of thrombus. As a liquid-gas phase transition (PT) agent, PFH transforms from liquid phase to gas phase after irradiation with low-intensity focused ultrasound (LIFU), allowing for both US imaging and thrombolysis (Figure 4E) [83]. Thirty minutes after LIFU irradiation, compared with Fe_3O_4-PLGA-CREKA (NPT group), the DTE of Fe_3O_4-PLGA-PFH-CREKA (PT group) in B mode and CEUS mode increased by 12-fold and 6.6-fold, respectively, indicating that the modification of PFH endowed the Fe_3O_4-PLGA-PFH-CREKA with excellent US imaging capability (Figure 4F,G). Therefore, Fe_3O_4-PLGA-PFH-CREKA was used to monitor thrombolytic effects *in vivo*. Fifteen minutes after intravenous injection, the DTE of the PT group in B mode and CEUS mode were significantly higher than that in NPT and sham (saline injection) groups, suggesting that the modification of PFH facilitated the liquid-gas transition function of Fe_3O_4-PLGA-PFH-CREKA NPs, which in turn improved US imaging and thrombolysis (Figure 4H,J). Fe_3O_4-PLGA-PFH-CREKA NPs exhibited excellent US imaging performance and thrombolytic effect, which realized imaging-guided therapy. These results demonstrated that nanoprobe-based US imaging broke through the limitations of previous poor resolution and enabled the diagnosis of CVD at the molecular level.

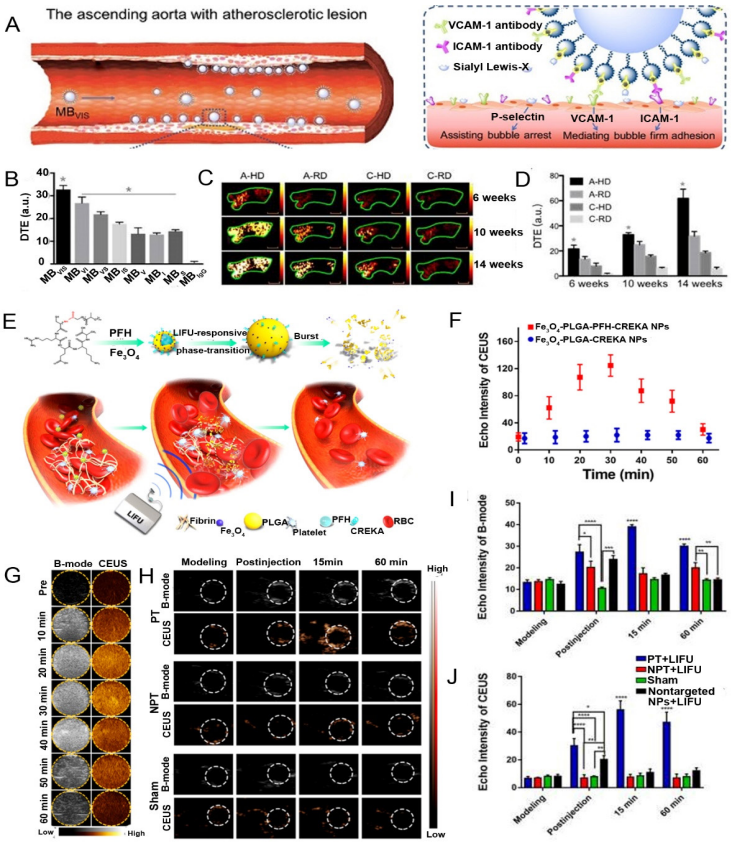

Figure 4. (A) Schematic illustration of MB_{VIS}. (B) US signal intensity of different NPs. (C) US images of different mice treated with MB_{VIS}. (D) Quantitative analysis of US signal. A-HD: $ApoE^{-/-}$ mice were fed a high-fat diet. A-RD: $ApoE^{-/-}$ mice were fed a regular diet. C-HD: C57BL/6 mice were fed a high-fat diet. C-RD: C57BL/6 mice were fed a regular diet. (E) Schematic illustration of Fe_3O_4-PLGA-PFH-CREKA. (F) Echo intensity of different NPs after LIFU irradiation. (G) CEUS and B-mode images of the PT process of the Fe_3O_4-PLGA-PFH-CREKA NPs. (H) US images of rat aorta at different time points after different NPs treatments. PT group: Fe_3O_4-PLGA-PFH-CREKA NPs. NPT group: Fe_3O_4-PLGA-CREKA NPs. Sham group: saline. (I) Quantification of grayscale intensity for B-mode. (J) Quantification of grayscale intensity for CEUS. (A-D) Reproduced with permission [82]. Copyright 2018, Ivyspring International Publisher. (E-J) Reproduced with permission [83]. Copyright 2019, American Chemical Society.

1.5 Computed tomography

Computed tomography (CT) utilizes X-rays to get cross-sectional images and anatomical details, and is one of the most frequently used imaging means because of its non-invasiveness, high spatial resolution, and low cost [84-86]. With the help of iodine-based compound contrast agents, clinical CT can distinguish different tissue structures via electron densities. The development of nanoprobes-based CT contrast agents showed a great potential for molecular imaging of CVD [87-90]. For example, Vyavahare et al. reported a degraded elastin-targeted NPs (EL-GNP) consisting of gold NPs (GNPs) as contrast agents and elastin antibodies as targeting agents for CT imaging of abdominal aortic aneurysms (Figure 5A) [91]. After retro-orbital injection, both the 3D model (left) and the attenuation pattern (right) showed higher contrast intensity in the aneurysm area than that in the healthy area because of the elastin antibodies with excellent targetability contributed to the accumulation of EL-GNP in the aneurysm area (Figure 5B). Therefore, the signal intensity of EL-GNP gradually decreased with the decrease of aortic elastin expression (elastin expression: A1>A2>A3>A4) (Figure 5C). Furthermore, the signal intensity of EL-GNP was negatively correlated with rupture pressure (Figure 5D). These results demonstrated that EL-GNP could locate the aneurysm accurately and reflect the rupture pressure through the signal intensity, which contributed to assessing the risk of aneurysm rupture.

The low spatial resolution of conventional CT does not differentiate between arterial wall calcification. NPs-based photon-counting CT (PCCT) quantifies the energy of individual photons in the structures in the form of K-edge imaging, improving spatial resolution [92, 93]. For instance, Si-Mohamed and co-workers reported GNPs as a PCCT contrast agent for K-edge imaging of macrophages in atherosclerotic plaques (Figure 5E) [94]. Compared with conventional imaging, in vitro K-edge imaging depicted only the GNPs tube, with no background or signal from the iodine and calcium tubes, indicating PCCT can specifically image GNPs (Figure 5F). After two days of intravenous injection, GNPs were enriched around the calcified areas of plaques, endowing more pronounced K-edge images as compared to conventional CT imaging, confirming the superiority of PCCT in diagnosing plaques (Figure 5G, H). Furthermore, the concentration of GNPs showed a positive linear correlation with the macrophage area within the plaque, indicating that PCCT could quantify the macrophages (Figure 5I). GNPs-based PCCT could reflect the degree of plaque lesions by quantifying macrophages, possessing a better diagnostic effect than conventional CT imaging.

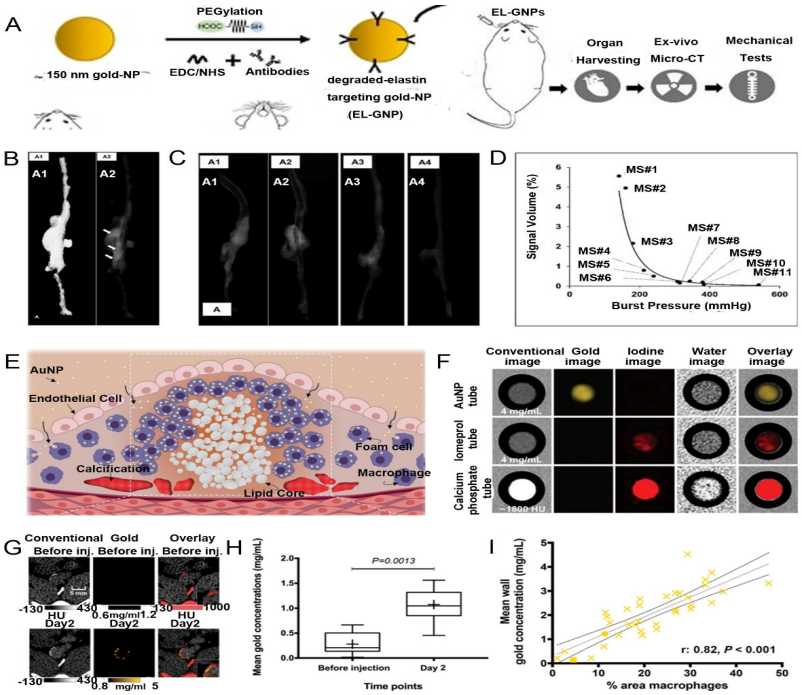

Figure 5. (A) Schematic illustration of EL-GNP. (B) Aneurysm aorta in attenuation mode (A1). Distribution of EL-GNP in the aorta (A2). (C) 3D aorta models were reconstructed in attenuation mode for MS#1 (A1), MS#5 (A2), MS#11(A3), and control mice (A4). (D) Graph of the relationship between signal strength and burst pressure. (E) Schematic illustration of gold NPs. (F) PCCT images of different materials. (G) PCCT images of non-calcified (top) and calcified (bottom) areas. (H) Gold NPs concentrations before and after injection. (I) Plot of macrophage area versus gold NPs concentration. (A-D) Reproduced with permission [91]. Copyright 2019, Ivyspring International Publisher. (E-I) Reproduced with permission [94]. Copyright 2021, Radiological Society of North America.

1.6 Multimodal imaging

CVDs have complex pathological mechanisms with high concealment and irreversibility, which brings a great challenge to treatment and diagnosis of disease [95, 96]. Nevertheless, a single imaging technique cannot provide all the information required [97-100]. For example, MRI has high spatial resolution with low sensitivity. PA imaging has high sensitivity without effective tissue penetration. Multimodal imaging can provide more detailed information about the efficacy of treatment compared to single imaging. For instance, Ran et al. reported a multimodal imaging NPs (PHPMR NPs) consisting of perfluoropentane (PFP) as US contrast agents, hematoporphyrin monomethylether (HMME) as sonosensitizers, polylacticacid-glycolic acids (PLGA) as plaque targeting agents, manganese ferrite ($MnFe_2O_4$) as MR/PA contrast agents and ramucirumab as plaque neovascularization inhibitors for the theranostics of AS (Figure 6A) [101]. The PHPMR NPs possessed the potential for PA/MR/US imaging due to their broad UV–vis–NIR absorption, paramagnetic properties, and LIFU-stimulated liquid-gas transition properties. As shown in Figure 6B, the MR signals gradually increased as a function of the Mn+Fe concentration, and the relaxation rate r_1 and r_2 of the PHPMR NPs were calculated to be 7.728 and 16.4 mM^{-1} s^{-1}, respectively, resulting in r_2/r_1 to be 2.12, confirming exceptional MR imaging capability of the PHPMR NPs. Furthermore, the PA signal of PHPMR NPs was higher than that of the $MnFe_2O_4$-free group and increased with the concentration, demonstrating that the PHPMR NPs had excellent PA imaging capability (Figure 6C). In addition, after LIFU irradiation, the DTE reached a maximum value at 4 min post-irradiation, indicating good US imaging capability of the PHPMR NPs (Figure 6D). After intravenous injection, compared to the Ram-free and $MnFe_2O_4$-free groups, the PHPMR NPs group exhibited higher T_1 and PA signals at 90 min and higher echo signals after LIFU irradiation, confirming the more robust MR/PA/US imaging performance of PHPMR NPs (Figure 6E, F). PHPMR-based multimodal imaging had the soft tissue resolution of MRI, the high sensitivity of PA imaging, and the tissue penetration of US imaging, which contributed to subsequent imaging-guided treatment.

In another example, Cao and co-workers prepared a PEGylated Fe_3O_4 NPs (FITC-LASG-PEGylated Fe_3O_4 NP) with a fluorescent dye (FITC) attached to its surface by thrombin-sensitive peptide (LASG) for FL/MR dual-imaging of thrombus (Figure 6G) [102]. Based on the principle that quenching occurred when FITC was attached to the Fe_3O_4 NPs surface, after LASG was specifically cleaved by thrombin, FITC left the Fe_3O_4 NPs and emitted FL. The enhancement of the T_1-weighted MRI signal increased in a concentration-dependent manner of Fe ions in FITC-LASG-PEGylated Fe_3O_4 NPs (Figure 6H). Furthermore, the FL intensity of FITC-LASG-PEGylated Fe_3O_4 NPs increased with increasing thrombin concentration. These results confirmed the MR imaging and thrombin-activatable FL imaging capabilities of FITC-LASG-PEGylated Fe_3O_4 NPs (Figure 6I). After intravenous injection, the thrombus group exhibited stronger FL (Figure 6J,K) and MR signals than the other groups due to thrombin enrichment, indicating that FITC-LASG-PEGylated Fe_3O_4 NPs accurately diagnose thrombus by FL imaging and MR imaging. These results illustrated that nanoprobe-based multimodal imaging could significantly avoid the defects of single imaging and improve imaging sensitivity and spatial resolution, thereby confirming the potential for CVD diagnosis.

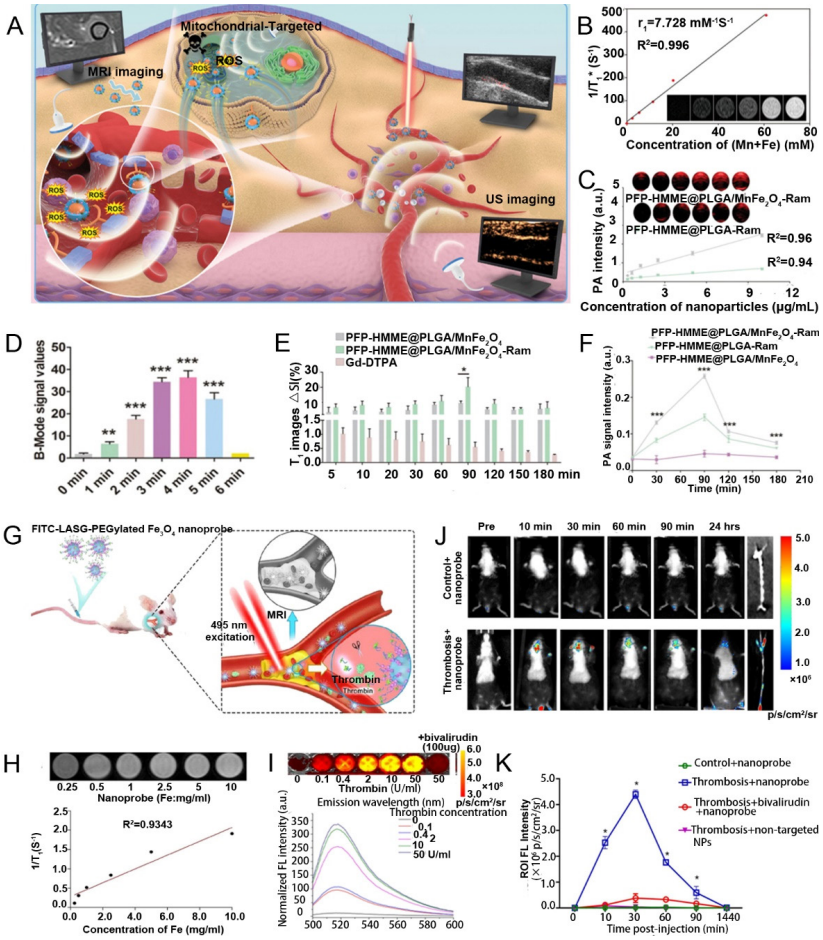

Figure 6. (A) Schematic illustration of PHPMR NPs. (B) MRI T_1 images of PHPMR under different Mn+Fe concentrations. (C) PA images at various concentrations of the two NPs. (D) Echo intensity of PHPMR at different time points after LIFU irradiation. (E) MRI T_1 signal intensities of different NPs within rabbits' plaque. (F) PA signal intensities of different NPs within rabbits' plaque. (G) Schematic illustration of FITC-LASG-PEGylated Fe_3O_4 NP. (H) T1WI MRI of different concentrations of the FITC-LASG-PEGylated Fe_3O_4 nanoprobe. (I) Fluorescence emission spectra of the nanoprobe at different concentrations of thrombin. (J) Fluorescence images of mice treated with different NPs. (K) Fluorescence intensity of mice treated with different NPs. (A-F) Reproduced with permission [101]. Copyright 2021, Wiley-VCH. (G-K) Reproduced with permission [102]. Copyright 2021, American Chemical Society.

Table 1. The merits and drawbacks of different imaging modalities

Classification	Merits	Drawbacks
FL imaging	high spatial resolution; high sensitivity; low cost; nonionizing radiation	moderate penetration depth; pre-clinical
PA imaging	high sensitivity; superior penetration depths compared with FL imaging; real-time; nonionizing radiation	poor penetration depths when compared with MR imaging; pre-clinical
MR imaging	good spatial resolution; non-invasion; high soft tissue contrast; nonionizing radiation	poor sensitivity; poor signal to noise ratio; long imaging times
US imaging	low cost; good sensitivity; real-time; nonionizing radiation	poor signal to noise ratio; poor penetration
CT imaging	non-invasion; good spatial resolution; fast imaging	low sensitivity; ionizing radiation; poor soft tissue contrast
Multimodal imaging	high sensitivity; high penetration depths; high speed real-time imaging; high spatial resolution	the technology is immature and in its infancy; pre-clinical

2. Conclusions and perspectives

The pathogenesis of CVD is complex and involves both hemodynamic and non-hemodynamic mechanisms, which is significantly different from other diseases. Nanoprobes-based molecular imaging seems particularly important for CVD diagnosis, because various imaging modalities have the advantage of safely, sensitively, and accurately diagnosing CVD at the molecular level via utilizing nanoprobes as imaging agents, providing vital information on the structure, function, metabolism, and genetic variation of diseased tissues [103-105]. Various nanoprobes were explored for molecular imaging in the past few years.

Here, we introduced different molecular imaging concepts and features, focusing on the recent applications of nanoprobes-based molecular imaging in CVD. With the further development of nanomedicine, the application of molecular imaging in CVD will become more and more extensive. To date, research on nano-imaging agents has mainly focused on two aspects: first, the improvement and optimization of existing contrast agents combined with multifunctionality; second, the development of novel contrast agents that are more powerful than previous contrast agents.

Although various nanoprobes-based molecular imaging has been reported in CVD in recent years, the research of nano-imaging agents is still far from clinical application. While nano-imaging agents achieve a molecular-level diagnosis, they also expose some problems, such as poor biocompatibility, large doses, low targeting, and difficulty in quantitative evaluation [106-108]. Therefore, it is still necessary to further optimize the role of nanoprobes in molecular imaging. Future research should focus on the following aspects: 1. improving the properties of contrast agents, taking fluorescent agents as an example, optimizing FL excitation and absorption wavelengths; 2. using biomimetic technologies to improve the biocompatibility of nanoprobes, such as coating NPs with platelet membranes or red blood cell membranes; 3. changing shape and bonding way of nanomaterials to increase efficiency, such as increasing targeted modification and changing the aspect ratio of nanorods. Therefore, biomimetic nanomaterials with unique optical, acoustic, or magneto-mechanical properties have become a hotspot in molecular imaging research. In conclusion, we believe that with the development of science and technology, the research of nanomaterials in molecular imaging will continue to deepen, which will help the application of molecular imaging in the diagnosis of various diseases, including CVD.

Disclosure

The authors declare no conflict of interest.

Authors' contributions

C. Wei. and Y. Wang. wrote the first draft, P. Li. and Q. Fu. provided fund support, Q. Fu designed the scheme as well as revised and supervised the manuscript. All authors approved the manuscript.

Acknowledgements

This work was supported by National Natural Science Foundation of China (Grant Number: 91849209), and Grants for Scientific Research of Distinguished Professor from Qingdao University, China (Grant Number: DC2200000953).

References

[1] Leong D., Joseph P., McKee M., et al. Reducing the Global Burden of Cardiovascular Disease, Part 2: Prevention and Treatment of Cardiovascular Disease. *Circulation Research*. 2017;121(6): 695-710. doi:https://doi.org/10.1161/CIRCRESAHA.117.311849.

[2] Soppert J., Lehrke M., Marx N., et al. Lipoproteins and Lipids in Cardiovascular Disease: from Mechanistic Insights to Therapeutic Targeting. *Advanced Drug Delivery Reviews*. 2020;159: 4-33. doi:https://doi.org/10.1016/j.addr.2020.07.019.

[3] Kim A. and Conte MS. Specialized Pro-Resolving Lipid Mediators in Cardiovascular Disease, Diagnosis, and Therapy. *Advanced Drug Delivery Reviews.* 2020;159: 170-179. doi:https://doi.org/10.1016/j.addr.2020.07.011.

[4] Roger V., Sidney S., Fairchild A., et al. Recommendations for Cardiovascular Health and Disease Surveillance for 2030 and Beyond: A Policy Statement From the American Heart Association. *Circulation.* 2020;141(9): 104-119. doi:https://doi.org/10.1161/CIR.0000000000000756.

[5] Shen C. and Ge J. Epidemic of Cardiovascular Disease in China: Current Perspective and Prospects for the Future. *Circulation*. 2018;138(4): 342-344. doi:https://doi.org/10.1161/CIRCULATIONAHA.118.033484.

[6] Iida M., Harada S., and Takebayashi T. Application of Metabolomics to Epidemiological Studies of Atherosclerosis and Cardiovascular Disease. *Journal of Atherosclerosis and Thrombosis*. 2019;26(9): 747-757. doi:https://doi.org/10.5551/jat.RV17036.

[7] Frostegård J. Immunity, Atherosclerosis and Cardiovascular Disease. *BMC Medicine*. 2013;11: 117. doi:https://doi.org/10.1186/1741-7015-11-117.

[8] Ouimet M., Barrett T., and Fisher EA. HDL and Reverse Cholesterol Transport. *Circulation Research*. 2019;124(10): 1505-1518. doi:https://doi.org/10.1161/

CIRCRESAHA.119.312617.
[9] Vasan R., Pan S, Larson M., et al. Arteriosclerosis, Atherosclerosis, and Cardiovascular Health: Joint Relations to the Incidence of Cardiovascular Disease. *Hypertension*. 2021;78(5): 1232-1240. doi:https://doi.org/10.1161/HYPERTENSIONAHA.121.18075.
[10] Zhao D., Liu J., Wang M., et al. Epidemiology of Cardiovascular Disease in China: Current Features and Implications. *Nature Reviews Cardiology*. 2019;16(4): 203-212. doi:https://doi.org/10.1038/s41569-018-0119-4.
[11] Lyngbakken M., Myhre P., Røsjø H., et al. Novel Biomarkers of Cardiovascular Disease: Applications in Clinical Practice. *Critical Reviews in Clinical Laboratory Sciences*. 2019;56(1): 33-60. doi:https://doi.org/10.1080/10408363.2018.1525335.
[12] Lu D. and Thum T. RNA-based Diagnostic and Therapeutic Strategies for Cardiovascular Disease. *Nature Reviews Cardiology*. 2019;16(11): 661-674. doi:https://doi.org/10.1038/s41569-019-0218-x.
[13] Jansen F., Nickenig G., and Werner N. Extracellular Vesicles in Cardiovascular Disease: Potential Applications in Diagnosis, Prognosis, and Epidemiology. *Circulation Research.* 2017;120(10): 1649-1657. doi:https://doi.org/10.1161/CIRCRESAHA.117.310752.
[14] Celermajer D., Chow C., Marijon E, et al. Cardiovascular Disease in the Developing World: Prevalences, Patterns, and the Potential of Early Disease Detection. *Journal of the American College of Cardiology*. 2012;60(14): 1207-1216. Available from:https://www.jacc.org/doi/abs/10.1016/j.jacc.2012.03.074.
[15] Bengel F. Clinical Cardiovascular Molecular Imaging. *Journal of Nuclear Medicine*. 2009;50(6): 837-840. doi:https://doi.org/10.2967/jnumed.108.059246.
[16] Wang X., Zhang F., Zhang C., et al. The Biomarkers for Acute Myocardial Infarction and Heart Failure. *BioMed Research International*. 2020;2020: 2018035. doi:https://doi.org/10.1155/2020/2018035.
[17] Barstow C., Rice M., and McDivitt J. Acute Coronary Syndrome: Diagnostic Evaluation. *American Family Physician*. 2017;95(3): 170-177. Available from:https://www.aafp.org/pubs/afp/issues/2017/0201/p170.html.
[18] Wesselius F., van S., De G., et al. Digital Biomarkers and Algorithms for Detection of Atrial Fibrillation using Surface Electrocardiograms: A Systematic Review. *Computers in Biology and Medicine.* 2021;133: 104404. doi:https://doi.org/10.1016/j.compbiomed.2021.104404.
[19] McGarry M. and Shenvi C. Identification of Acute Coronary Syndrome in the Elderly. *Emergency Medicine Clinics of North America.* 2021;39(2): 339-346. doi:https://doi.org/10.1016/j.emc.2020.12.003.
[20] Clerico A., Zaninotto M., Padoan A., et al. Evaluation of Analytical Performance of Immunoassay Methods for cTnI and cTnT: From theory to practice. *Advances in Clinical Chemistry*. 2019;93: 239-262. doi:https://doi.org/10.1016/bs.acc.2019.07.005.
[21] Ma H., Cassedy A., O'Kennedy R.. The Role of Antibody-based Troponin Detection in Cardiovascular Disease: A Critical Assessment. *Journal of Immunological Methods.* 2021;497: 113108. doi:https://doi.org/10.1016/j.jim.2021.113108.
[22] Duque-Ossa L., García-Ferrera B., and Reyes-Retana J. Troponin I as a Biomarker for Early Detection of Acute Myocardial Infarction. *Current Problems in Cardiology.* 2021: 101067. doi:https://doi.org/10.1016/j.cpcardiol.2021.101067.
[23] Fathil M., Md A., Gopinath S., et al. Diagnostics on Acute Myocardial Infarction: Cardiac Troponin Biomarkers. *Biosensors & Bioelectronics.* 2015;70: 209-220. doi:https://doi.org/10.1016/j.bios.2015.03.037.
[24] Finocchiaro G, Sheikh N, Biagini E, et al. The Electrocardiogram in the Diagnosis and Management of Patients with Hypertrophic Cardiomyopathy. *Heart Rhythm*. 2020;17(1): 142-151. doi:https://doi.org/10.1016/j.hrthm.2019.07.019.
[25] Hornick J., Costantini O. The Electrocardiogram: Still a Useful Tool in the Primary Care Office. *The Medical Clinics of North America*. 2019;103(5): 775-784. doi:https://doi.org/10.1016/j.mcna.2019.04.003.
[26] Jin Z, Dong A, Shu M., et al. Sparse ECG Denoising with Generalized Minimax Concave Penalty. *Sensors.* 2019;19(7): 1718. doi:https://doi.org/10.3390/s19071718.
[27] Luz E., Schwartz W., Cámara-Chávez G., et al. ECG-based Heartbeat Classification for Arrhythmia Detection: A Survey. *Computer Methods and Programs in Biomedicine*. 2016;127: 144-164. doi:https://doi.org/10.1016/j.cmpb.2015.12.008.
[28] Rozanski A., Muhlestein J., and Berman DS. Primary Prevention of CVD: The Role of Imaging Trials. *JACC Cardiovasc Imaging*. 2017;10(3): 304-317. Available from:https://www.jacc.org/doi/abs/10.1016/j.jcmg.2017.01.009.
[29] Masri A., Bukhari S., Eisele Y., et al. Molecular Imaging of Cardiac Amyloidosis. *Journal of Nuclear Medicine.* 2020;61(7): 965-970. doi:https://doi.org/10.2967/jnumed.120.245381.
[30] Farber G., Boczar K., Wiefels CC., et al. The Future of Cardiac Molecular Imaging. *Seminars in Nuclear Medicine.* 2020;50(4): 367-385. doi:https://doi.org/10.1053/j.semnuclmed.2020.02.005.
[31] Brown E, Lindner JR. Ultrasound Molecular Imaging: Principles and Applications in Cardiovascular Medicine. *Current Cardiology Reports*. 2019;21(5): 30. doi:https://doi.org/10.1007/s11886-019-1117-9.
[32] Li H., Chen Y., Jin Q., et al. Noninvasive Radionuclide Molecular Imaging of the CD4-Positive T Lymphocytes in Acute Cardiac Rejection. *Molecular Pharmaceutics*. 2021;18(3): 1317-1326. doi:https://doi.org/10.1021/acs.molpharmaceut.0c01155.
[33] Ahmed M., Tegnebratt T., Tran T., et al. Molecular Imaging of Inflammation in a Mouse Model of

Atherosclerosis Using a Zirconium-89-Labeled Probe. *International Journal of Nanomedicine.* 2020;15: 6137-6152. doi:https://doi.org/10.2147%2FIJN.S256395.

[34] Varasteh Z., Mohanta S., Robu S., et al. Molecular Imaging of Fibroblast Activity After Myocardial Infarction Using a 68Ga-Labeled Fibroblast Activation Protein Inhibitor, FAPI-04. *Journal of Nuclear Medicine.* 2019;60(12): 1743-1749. doi:https://doi.org/10.2967/jnumed.119.226993.

[35] Wang X., Ziegler M., McFadyen J., et al. Molecular Imaging of Arterial and Venous Thrombosis. *British Journal of Pharmacology.* 2021; 178(21): 4246-4269. doi:https://doi.org/10.1111/bph.15635.

[36] Anderson C., and Lewis J. Current Status and Future Challenges for Molecular Imaging. *Philosophical Transactions of the Royal Society A: Mathematical, Physical and Engineering Sciences*. 2017;375: 20170023. doi:https://doi.org/10.1098/rsta.2017.0023

[37] Wang X., Peter K.. Molecular Imaging of Atherothrombotic Diseases: Seeing Is Believing. *Arteriosclerosis, thrombosis, and vascular biology*. 2017;37(6): 1029-1040. doi:https://doi.org/10.1161/ATVBAHA.116.306483.

[38] Larivière M., Bonnet S., Lorenzato C., et al. Recent Advances in the Molecular Imaging of Atherosclerosis. *Seminars in Thrombosis and Hemostasis*. 2020;46(5): 563-586. doi:10.1055/s-0039-1701019.

[39] Li Y., Chen Y., Du M., et al. Ultrasound Technology for Molecular Imaging: From Contrast Agents to Multimodal Imaging. *ACS Biomaterials Science & Engineering*. 2018; 4(8): 2716-2728. doi:https://doi.org/10.1021/acsbiomaterials.8b00421.

[40] Zhang X., Wu M., Zhang Y., et al. Molecular Imaging of Atherosclerotic Plaque with Lipid Nanobubbles as Targeted Ultrasound Contrast Agents. *Colloids and Surfaces B, Biointerfaces.* 2020;189: 110861. doi:https://doi.org/10.1016/j.colsurfb.2020.110861.

[41] Laramie M., Smith M., Marmarchi F., et al. Small Molecule Optoacoustic Contrast Agents: An Unexplored Avenue for Enhancing In Vivo Imaging. *Molecules*. 2018; 23(11): 2766. doi:https://doi.org/10.3390/molecules23112766.

[42] Meng Q., Wu M., Shang Z., et al. Responsive Gadolinium(III) Complex-based Small Molecule Magnetic Resonance Imaging Probes: Design, Mechanism and Application. *Coordination Chemistry Reviews.* 2022;457: 214398. doi:https://doi.org/10.1016/j.ccr.2021.214398.

[43] Zhu J., Sun W., and Shi X. Nanogels as Contrast Agents for Molecular Imaging. *Chinese Journal of Chemistry.* 2016;34(6): 547-557. doi:https://doi.org/10.1002/cjoc.201500743.

[44] Zhou J., Guo D., Zhang Y., et al. Construction and Evaluation of Fe_3O_4-based PLGA Nanoparticles Carrying rtPA used in the Detection of Thrombosis and in Targeted Thrombolysis. *ACS Applied Materials & interfaces*. 2014;6(8): 5566-5576. doi:https://doi.org/10.1021/am406008k.

[45] Tuguntaev R., Hussain A., Fu C., et al. Bioimaging Guided Pharmaceutical Evaluations of Nanomedicines for Clinical Translations. *Journal of Nanobiotechnology*. 2022;20(1): 236. doi:https://doi.org/10.1186/s12951-022-01451-4.

[46] Chan C., Zhang L., Cheng C., et al. Recent Advances in Managing Atherosclerosis via Nanomedicine. *Small*. 2018;14(4):1702793. doi:https://doi.org/10.1002/smll.201702793.

[47] Wang S., Ren W., Hou J., et al. Fluorescence Imaging of Pathophysiological Microenvironments. *Chemical Society Reviews*. 2021; 50(16): 8887-8902. doi:https://doi.org/10.1039/D1CS00083G.

[48] Bourantas C., Crake T., Zhang Y., et al. Intravascular Imaging in Cardiovascular Ageing. *Experimental Gerontology.* 2018;109: 31-37. doi:https://doi.org/10.1016/j.exger.2017.05.011.

[49] Zhang M., Chen J., Wang M., et al. Pyrene-Based Nonwoven Fabric with Tunable Fluorescence Properties by Employing the Aggregation-Caused Quenching Effect. *ACS Applied Materials & Interfaces*. 2021;13(7): 9036-9042. doi:https://doi.org/10.1021/acsami.0c23132.

[50] Li Q., Jia Y., Feng Z., et al. A Highly Sensitive and Selective Fluorescent Probe without Quencher for Detection of Pb^{2+} Ions Based on Aggregation-Caused Quenching Phenomenon. *RSC Advances*. 2018;8(68): 38929-38934. doi:https://doi.org/10.1039/C8RA07903J.

[51] Zhao Y., Zhu W., Ren L., et al. Aggregation-Induced Emission Polymer Nanoparticles with pH-responsive Fluorescence. *Polymer Chemistry*. 2016;7(34): 5386-5395. doi:https://doi.org/10.1039/C6PY01009A.

[52] Feng X., Qi C., Feng H-T., et al. Dual Fluorescence of Tetraphenylethylene-Substituted Pyrenes with Aggregation-Induced Emission Characteristics for White-Light Emission. *Chemical Science*. 2018;9(25): 5679-5687. doi:https://doi.org/10.1039/C8SC01709C.

[53] Xu H., She P., Ma B., et al. ROS Responsive Nanoparticles Loaded with Lipid-Specific AIEgen for Atherosclerosis-Targeted Diagnosis and Bifunctional Therapy. *Biomaterials*. 2022;288: 121734. doi:https://doi.org/10.1016/j.biomaterials.2022.121734.

[54] Ye Z., Ji M., Wu K., et al. In-Sequence High-Specificity Dual-Reporter Unlocking of Fluorescent Probe Enables the Precise Identification of Atherosclerotic Plaques. *Angewandte Chemie International Edition*. 2022;61(29): e202204518. doi:https://doi.org/10.1002/anie.202204518.

[55] Steinberg I., Huland D., Vermesh O., et al. Photoacoustic Clinical Imaging. *Photoacoustics*. 2019;14: 77-98. doi:https://doi.org/10.1016/j.pacs.2019.05.001.

[56] Attia A., Balasundaram G., Moothanchery M., et al. A review of Clinical Photoacoustic Imaging: Current and Future Trends. *Photoacoustics*. 2019;16: 100144.

doi:https://doi.org/10.1016/j.pacs.2019.100144.
[57] Wu M., Awasthi N., Rad N., et al. Advanced Ultrasound and Photoacoustic Imaging in Cardiology. *Sensors.* 2021;21(23): 7947. doi:https://doi.org/10.3390/s21237947.
[58] Gröhl J., Schellenberg M., Dreher K., et al. Deep Learning for Biomedical Photoacoustic Imaging: A review. *Photoacoustics*. 2021;22: 100241. doi:https://doi.org/10.1016/j.pacs.2021.100241.
[59] Fu Q., Zhu R., Song J., et al. Photoacoustic Imaging: Contrast Agents and Their Biomedical Applications. *Advanced Materials.* 2019;31(6): e1805875. doi:https://doi.org/10.1002/adma.201805875.
[60] Upputuri P., and Pramanik M. Recent Advances in Photoacoustic Contrast Agents for In Vivo Imaging. *Wiley Interdisciplinary Reviews Nanomedicine and nanobiotechnology*. 2020;12(4): e1618. doi:https://doi.org/10.1002/wnan.1618.
[61] Han S., Lee D., Kim S., et al. Contrast Agents for Photoacoustic Imaging: A Review Focusing on the Wavelength Range. *Biosensors*. 2022;12(8): 594. doi:https://doi.org/10.3390/bios12080594.
[62] Sivasubramanian M., and Lo L.. Assessment of Nanoparticle-Mediated Tumor Oxygen Modulation by Photoacoustic Imaging. *Biosensors.* 2022;12(5): 336. doi:https://doi.org/10.3390/bios12050336.
[63] Ge X., Cui H., Kong J., et al. A Non-Invasive Nanoprobe for In Vivo Photoacoustic Imaging of Vulnerable Atherosclerotic Plaque. *Advanced Materials.* 2020;32(38): 2000037. doi:https://doi.org/10.1002/adma.202000037.
[64] Huang X., Song J., Yung B., et al. Ratiometric Optical Nanoprobes enable Accurate Molecular Detection and Imaging. *Chemical Society Reviews*. 2018;47(8): 2873-2920. doi:https://doi.org/10.1039/C7CS00612H
[65] Liu Y., Teng L., Lyu Y., et al. Ratiometric afterglow Luminescent Nanoplatform Enables Reliable Quantification and Molecular Imaging. *Nature Communications*. 2022;13(1): 2216. doi:https://doi.org/10.1038/s41467-022-29894-1.
[66] Ma Y., Xu L., Yin B., et al. Ratiometric Semiconducting Polymer Nanoparticle for Reliable Photoacoustic Imaging of Pneumonia-Induced Vulnerable Atherosclerotic Plaque in Vivo. *Nano Letters.* 2021;21(10): 4484-4493. doi:https://doi.org/10.1021/acs.nanolett.1c01359.
[67] Han Y., Chen Y., Ferrari V. Contemporary Application of Cardiovascular Magnetic Resonance Imaging. *Annual Review of Medicine.* 2020;71(1): 221-234. doi:https://doi.org/10.1146/annurev-med-041818-015923.
[68] Wüst R., Calcagno C., Daal M., et al. Emerging Magnetic Resonance Imaging Techniques for Atherosclerosis Imaging. *Arteriosclerosis, Thrombosis, and Vascular Biology.* 2019;39(5): 841-849. doi:https://doi.org/10.1161/ATVBAHA.118.311756.
[69] Wang T., Ayoub C., Chetrit M., et al. Cardiac Magnetic Resonance Imaging Techniques and Applications for Pericardial Diseases. *Circulation: Cardiovascular Imaging.* 2022;15(7): e014283. doi:https://doi.org/10.1161/CIRCIMAGING.122.014283.
[70] Guo S., Li K., Hu B., et al. Membrane-destabilizing Ionizable Lipid Empowered Imaging-guided siRNA Delivery and Cancer Treatment. *Exploration.* 2021;1(1):35-49. doi:https://doi.org/10.1002/EXP.20210008.
[71] Sinharay S., and Pagel MD. Advances in Magnetic Resonance Imaging Contrast Agents for Biomarker Detection. *Annual Review of Analytical Chemistry.* 2016;9(1): 95-115. doi:https://doi.org/10.1146%2Fannurev-anchem-071015-041514.
[72] Bao Y., Sherwood J., and Sun Z. Magnetic Iron Oxide Nanoparticles as T1 Contrast Agents for Magnetic Resonance Imaging. *Journal of Materials Chemistry C*. 2018;6(6): 1280-1290. doi:https://doi.org/10.1039/C7TC05854C.
[73] Wei Q., Wang J., Shi W., et al. Improved In Vivo Detection of Atherosclerotic Plaques with a Tissue Factor-Targeting Magnetic Nanoprobe. *Acta Biomaterialia.* 2019;90: 324-336. doi:https://doi.org/10.1016/j.actbio.2019.04.014.
[74] Wu Y., Wu F., Liu Y., et al. High-Resolution Magnetic Resonance Imaging of Cervicocranial Artery Dissection. *Stroke*. 2019;50(11): 3101-3107. doi:https://doi.org/10.1161/STROKEAHA.119.026362.
[75] Phinikaridou A., Andia M., Saha P., et al. In Vivo Magnetization Transfer and Diffusion-Weighted Magnetic Resonance Imaging Detects Thrombus Composition in a Mouse Model of Deep Vein Thrombosis. *Circulation: Cardiovascular Imaging.* 2013;6(3): 433-440. doi:https://doi.org/10.1161/CIRCIMAGING.112.000077.
[76] Zhang Y., Cheng S., He Y., et al. Activated Platelet-Homing Nanoplatform for Targeting Magnetic Resonance Imaging of Aneurysm-Related Thrombus in Rabbits. *ACS Applied Materials & Interfaces.* 2021;13(43): 50705-50715. doi:https://doi.org/10.1021/acsami.1c13539.
[77] Heiles B., Terwiel D., and Maresca D. The Advent of Biomolecular Ultrasound Imaging. *Neuroscience.* 2021;474: 122-133. doi:https://doi.org/10.1016/j.neuroscience.2021.03.011.
[78] Dave J., Mc D., Mehrotra P., et al. Recent Technological Advancements in Cardiac Ultrasound Imaging. *Ultrasonics*. 2018;84: 329-340. doi:https://doi.org/10.1016/j.ultras.2017.11.013.
[79] Zamzmi G., Rajaraman S., Hsu L-Y., et al. Real-time Echocardiography Image Analysis and Quantification of Cardiac Indices. *Medical Image Analysis.* 2022;80: 102438. doi:https://doi.org/10.1016/j.media.2022.102438.
[80] Mehta KS., Lee J., Taha AA., et al. Vascular Applications of Contrast-Enhanced Ultrasound Imaging. *Journal of Vascular Surgery.* 2017;66(1): 266-274. doi:https://doi.org/10.1016/j.jvs.2016.12.133.
[81] Golemati S., and Cokkinos D. Recent Advances in Vascular Ultrasound Imaging Technology and their

clinical implications. *Ultrasonics*. 2022;119: 106599. doi:https://doi.org/10.1016/j.ultras.2021.106599.

[82] Yan F., Sun Y., Mao Y., et al. Ultrasound Molecular Imaging of Atherosclerosis for Early Diagnosis and Therapeutic Evaluation through Leucocyte-like Multiple Targeted Microbubbles. *Theranostics*. 2018;8(7): 1879-1891. doi:https://doi.org/10.7150%2Fthno.22070.

[83] Zhong Y., Zhang Y., Xu J., et al. Low-Intensity Focused Ultrasound-Responsive Phase-Transitional Nanoparticles for Thrombolysis without Vascular Damage: A Synergistic Nonpharmaceutical Strategy. *ACS Nano*. 2019;13(3): 3387-3403. doi:https://doi.org/10.1021/acsnano.8b09277.

[84] Aslan N., Ceylan B., Koç M., et al. Metallic Nanoparticles as X-Ray Computed Tomography (CT) Contrast Agents: A Review. *Journal of Molecular Structure*. 2020;1219: 128599. doi:https://doi.org/10.1016/j.molstruc.2020.128599.

[85] Mahan M., Doiron A. Gold Nanoparticles as X-Ray, CT, and Multimodal Imaging Contrast Agents: Formulation, Targeting, and Methodology. *Journal of Nanomaterials*. 2018;2018: 5837276. doi:https://doi.org/10.1155/2018/5837276.

[86] Diwakar M., and Kumar M. A Review on CT Image Noise and its Denoising. *Biomedical Signal Processing and Control.* 2018;42: 73-88. doi:https://doi.org/10.1016/j.bspc.2018.01.010.

[87] Liao W., Lei P., Pan J., et al. Bi-DTPA as a High-Performance CT Contrast Agent for In Vivo Imaging. *Biomaterials*. 2019;203: 1-11. doi:https://doi.org/10.1016/j.biomaterials.2019.03.001.

[88] Hernández-Rivera M., Kumar I., Cho S., et al. High-Performance Hybrid Bismuth–Carbon Nanotube Based Contrast Agent for X-ray CT Imaging. *ACS Applied Materials & Interfaces*. 2017;9(7): 5709-5716. doi:https://doi.org/10.1021/acsami.6b12768.

[89] Nieves L., Dong Y., Rosario-Berríos D., et al. Renally Excretable Silver Telluride Nanoparticles as Contrast Agents for X-ray Imaging. *ACS Applied Materials & Interfaces*. 2022;14(30): 34354-34364. doi:https://doi.org/10.1021/acsami.2c06190.

[90] Liu L., Gardecki J., Nadkarni S., et al. Imaging the Subcellular Structure of Human Coronary Atherosclerosis Using Micro–Optical Coherence Tomography. *Nature Medicine*. 2011;17(8):1010-1014. doi:https://doi.org/10.1038/nm.2409.

[91] Wang X., Lane B., Eberth J., et al. Gold Nanoparticles that Target Degraded Elastin Improve Imaging and Rupture Prediction in an AngII Mediated Mouse Model of Abdominal Aortic Aneurysm. *Theranostics*. 2019;9(14): 4156-4167. doi:https://doi.org/10.7150%2Fthno.34441.

[92] Li D., Zeng D., Li S., et al. MDM-PCCT: Multiple Dynamic Modulations for High-Performance Spectral PCCT Imaging. *IEEE Transactions on Medical Imaging*. 2020;39(11): 3630-3642. doi:10.1109/TMI.2020.3001616..

[93] Thomsen F., Horstmeier S., Niehoff J., et al. Effective Spatial Resolution of Photon Counting CT for Imaging of Trabecular Structures is Superior to Conventional Clinical CT and Similar to High Resolution Peripheral CT. *Investigative Radiology*. 2022;57(9): 620-626. doi:https://doi.org/10.1097/RLI.0000000000000873.

[94] Si-Mohamed S., Sigovan M., Hsu J., et al. In Vivo Molecular K-Edge Imaging of Atherosclerotic Plaque Using Photon-counting CT. *Radiology*. 2021;300(1): 98-107. doi:https://doi.org/10.1148/radiol.2021203968.

[95] Khoury M., Yang H., and Liu B. Macrophage Biology in Cardiovascular Diseases. *Arteriosclerosis, Thrombosis, and Vascular Biology.* 2021;41(2): e77-e81. doi:https://doi.org/10.1161/ATVBAHA.120.313584.

[96] Kietzmann T., Petry A., Shvetsova A., et al. The Epigenetic Landscape Related to Reactive Oxygen Species Formation in the Cardiovascular System. *British Journal of Pharmacology*. 2017;174(12): 1533-1554. doi:https://doi.org/10.1111/bph.13792.

[97] Ederhy S., Mansencal N,. Réant P., et al. Role of Multimodality Imaging in the Diagnosis and Management of Cardiomyopathies. *Archives of Cardiovascular Diseases.* 2019;112(10): 615-629. doi:https://doi.org/10.1016/j.acvd.2019.07.004.

[98] Güner A., Topel Ç., Cansever A., et al. Where is the Right Ventricle? Accurate Diagnosis with Cardiovascular Multimodality Imaging. *Echocardiography*. 2020;37(3): 456-461. doi:https://doi.org/10.1111/echo.14606.

[99] Xu M., Mao C., Chen H., et al. Osteopontin Targeted Theranostic Nanoprobes for Laser-induced Synergistic Regression of Vulnerable Atherosclerotic Plaques. *Acta Pharmaceutica Sinica B*. 2022;12(4): 2014-2028. doi:https://doi.org/10.1016/j.apsb.2021.12.020.

[100] Senders M., Hernot S., Carlucci G., et al. Nanobody-Facilitated Multiparametric PET/MRI Phenotyping of Atherosclerosis. *JACC: Cardiovascular Imaging.* 2019;12(10):2015-2026. Available from:https://www.jacc.org/doi/abs/10.1016/j.jcmg.2018.07.027.

[101] Yao J., Yang Z., Huang L., et al. Low-Intensity Focused Ultrasound-Responsive Ferrite-Encapsulated Nanoparticles for Atherosclerotic Plaque Neovascularization Theranostics. *Advanced Science*. 2021;8(19): e2100850. doi:https://doi.org/10.1002/advs.202100850.

[102] Wang Y., Xu M., Yang N., et al. A Thrombin-Responsive Nanoprobe for In Vivo Visualization of Thrombus Formation through Three-Dimensional Optical/Computed Tomography Hybrid Imaging. *ACS Applied Materials & Interfaces.* 2021;13(24): 27814-27824. doi:https://doi.org/10.1021/acsami.1c04065.

[103] Hu J., Ortgies D., Martín R., et al. Optical Nanoparticles

for Cardiovascular Imaging. *Advanced Optical Materials.* 2018;6(22): 1800626. doi:https://doi.org/10.1002/adom.201800626.
[104] Varna M., Xuan H., and Fort E. Gold Nanoparticles in Cardiovascular Imaging. *WIREs Nanomedicine and Nanobiotechnology*. 2018;10(1): e1470. doi:https://doi.org/10.1002/wnan.1470.
[105] Chen W., Schilperoort M., Cao Y., et al. Macrophage-Targeted Nanomedicine for the Diagnosis and Treatment of Atherosclerosis. *Nature Reviews Cardiology.* 2022;19(4): 228-249. doi:https://doi.org/10.1038/s41569-021-00629-x.
[106] Huang R., Zhou X., Chen G., et al. Advances of Functional Nanomaterials for Magnetic Resonance Imaging and Biomedical Engineering Applications. *WIREs Nanomedicine and Nanobiotechnology*. 2022;14(4): e1800. doi:https://doi.org/10.1002/wnan.1800.
[107] Chen J., Zhang X., Millican R., et al. Recent Advances in Nanomaterials for Therapy and Diagnosis for Atherosclerosis. *Advanced Drug Delivery Reviews*. 2021;170: 142-199. doi:https://doi.org/10.1016/j.addr.2021.01.005.
[108] Jamalipour S., and Iravani S. Eco-friendly and Sustainable Synthesis of Biocompatible Nanomaterials for Diagnostic Imaging: Current Challenges and Future Perspectives. *Green Chemistry.* 2020;22(9): 2662-2687. doi:https://doi.org/10.1039/D0GC00734J.

Author Biographies

Qinrui Fu is a distinguished professor and the director of the molecular treatment center at Institute for Translational Medicine, College of Medicine, Qingdao University, China; and a scientific research mentor at Key Laboratory of Birth Regulation and Control Technology of National Health Commission of China, Shandong Provincial Maternal and Child Health Care Hospital affiliated to Qingdao University. His research interests include molecular imaging probes, biomaterials, nano-assembly and drug delivery, and their various applications in biomedicine.